UL-HEP-94-1
SI-94-2
April 1994

Photoproduction within the two-component Dual Parton Model

1. Amplitudes and Cross Sections

R. Engel

Fachbereich Physik, Universität Leipzig, D-04109 Leipzig, Germany

and

Fachbereich Physik, Universität Siegen, D-57068 Siegen, Germany

Abstract

In the framework of the Dual Parton Model we present an approximation scheme to describe high energy photoproduction processes. Based on the distinction between direct, resolved soft, and resolved hard interaction processes we construct an effective impact parameter amplitude. In order to treat low mass diffraction within the eikonal formalism in a consistent way a phenomenological ansatz is proposed. The free parameters of the model are determined by fits to high energy photoproduction cross sections. We calculate the partial photoproduction cross sections and give predictions for HERA energies.

1 Introduction

The HERA collider allows the investigation of photoproduction processes at much higher energies than previously possible (for a general review see Ref. [1]). First data have already been published [2-6]. In this new energy range, soft particle production is strongly connected to hard scattering processes resulting in minijets. Several attempts have been made to understand photoproduction at HERA in these terms [7-12]. Although a number of models designed to give an almost complete description of photoproduction processes are described in the literature [13-18], a model based on the Dual Parton Model (DPM) has as yet not been presented. It is worthwhile investigating the predictions of this model for the following reasons.

Within the framework of the DPM (for a recent review see [19]) one can calculate both elastic processes (i.e. cross sections) and inelastic processes (i.e. multiparticle production) in a consistent way. The model relates the free parameters necessary to describe the cross sections directly to multiparticle production. Furthermore the DPM connects both soft and hard subprocesses by an unitarization scheme. This unified treatment of soft and hard processes is necessary because of the rapid increase of the minijet contribution at higher collision energies.

Previous studies have shown that the DPM successfully describes most features of high energy hadronic processes. For example the violation of Feynman scaling, the rise of the central rapidity plateau, long range correlations, violation of Koba-Nielsen-Olesen scaling, and multiplicity-transverse momentum correlations.

Furthermore we want to emphasize that diffraction plays an important role in inelastic photoproduction processes. This follows from the fact that the main contribution to photon-hadron scattering at low momentum transfer results from processes where the photon couples directly to virtual $q\bar{q}$ states. Therefore, elastic and inelastic corrections to the Born amplitude implied by unitarity cannot be neglected. To our knowledge no detailed photoproduction model involving inelastic absorptive corrections exists. In order to take these corrections into account we use a two-channel eikonal model to approximate low and high mass diffraction [20]. In this scheme we can describe the essential features of photoproduction while keeping the number of free parameters as small as possible.

Using the assumptions of the Dual Parton Model, a detailed model of both elastic and inelastic photoproduction processes is presented. Within this model, processes involving soft and hard interactions are considered. Furthermore, a self-consistent approximation giving effective amplitudes for elastic and inelastic photoproduction cross sections is discussed. The free parameters of the model are determined by a fit to photoproduction data and predictions for the partial cross sections at HERA energies are given. In a forthcoming paper [21], these amplitudes will be used in a Monte-Carlo event generator to investigate the model predictions for multiparticle production. There, the model will be compared to experimental data on photoproduction at an energy of $\sqrt{s} \approx 15$ GeV. Predictions for multiparticle production at HERA energies will be given.

The outline of this paper is as follows. In section 2 we discuss the resolved and direct interactions of photons with hadronic matter. In section 3 we present a general phenomenological treatment of low and high mass diffraction within the eikonal approximation. Based on the typical interaction processes and the assumptions of the Dual Parton Model, we construct, in section 4, an effective impact parameter amplitude to describe

photoproduction. In section 5 we determine the free parameters of the model by fits to high energy photoproduction cross sections and compare our results with measurements. In addition, predictions for HERA energies are given.

2 Classification of photon hadron interactions

In leading order perturbative QCD, the classification of photon interactions into direct and resolved processes is an efficient way of describing the dual nature of the photon. In this picture we consider the physical photon as a superposition of the *bare* photon and the *hadronic* photon.

The *hadronic* photon results from the fluctuations of the photon into $q\bar{q}$ pairs and the further development of this system. Due to the quantum numbers of the photon, it is expected that the $q\bar{q}$-pairs form particles with small masses like vector mesons or two pion states. In the framework of the vector meson dominance model (VDM) [22] the hadronic component of the photon consists of the three lightest vector mesons ρ^0, ω, and ϕ. As the collision energy is increased vector meson states with higher mass will enter the interaction. This is recognized in the generalized vector meson dominance model (GVDM) [23]. But there is also a nonvanishing probability that the photon couples directly to two pions [24]. As we cannot calculate this two pion contribution no standard method exists to correct experimental vector meson production cross sections for this background. To avoid the resulting ambiguities we neither distinguish between $q\bar{q}$ states and two pion states nor vector mesons. We use the mass of these fluctuations as an effective parameter to characterize the hadronic component of the photon. For definiteness we will restrict ourselves in the following discussion to photon proton collisions.

The *bare* photon interacts via *direct* processes, i.e. the photon participates directly in the scattering process. For interactions involving sufficiently large momentum transfer this direct contribution can be estimated by lowest order perturbative QCD,

$$\sigma_{dir}(s, p_\perp^{cutoff}) = \int dx \int d\hat{t} \sum_{i,k,l} \frac{1}{1+\delta_{k,l}} f_{p,i}(x, Q^2) \frac{d\sigma^{QCD}_{\gamma,i\to k,l}(\hat{s}, \hat{t})}{d\hat{t}}, \tag{1}$$

where $f_{p,i}(x, Q^2)$ denotes the parton distribution function of the proton for the parton i and the sum runs over all possible parton configurations i, k, l. The Mandelstam variables of the parton subprocesses are given by $\hat{s}$ and $\hat{t}$. The integrations over x and $\hat{t}$ are limited by the transverse momentum cutoff $p_\perp^{cutoff}$. Within the Parton Model only the two processes shown in figure 1 contribute.

The interactions of the *hadronic* component of the photon are called resolved processes. It is assumed that the photon fluctuates into a $q\bar{q}$ pair which interacts hadronically. This reduces the problem to the calculation of the interaction of $q\bar{q}$ states with hadrons, but currently this cannot be done from first principles. Therefore, we split this contribution into hard interactions and the remaining soft interactions. In order to distinguish between these two contributions we again use a transverse momentum cutoff $p_\perp^{cutoff}$. All the subprocesses involving transverse momenta greater than this scale are considered as hard. We estimate the contribution resulting from hard subprocesses again by lowest order

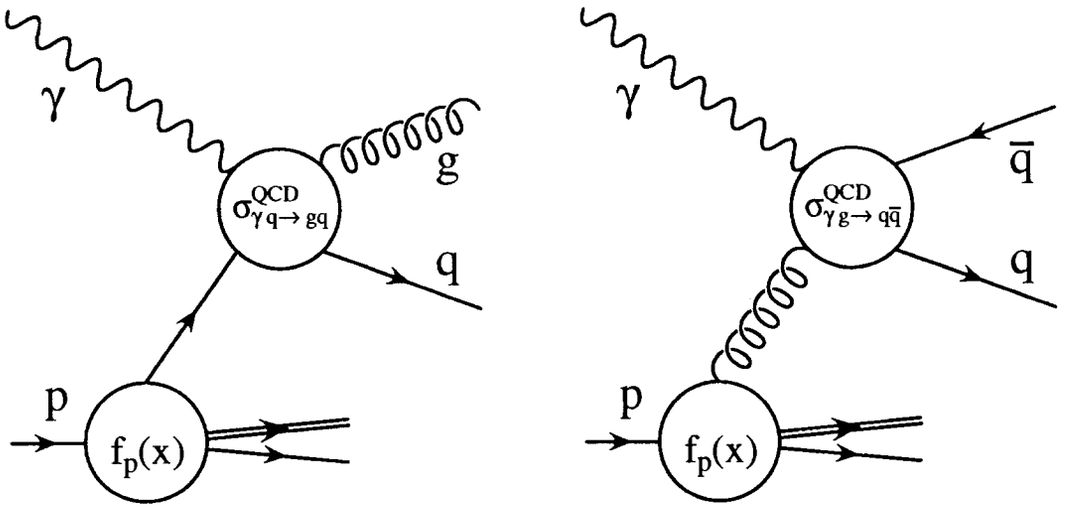

Figure 1: Direct processes contributing to $\gamma p \to X$ scattering: a) gluon Compton scattering, b) photon gluon fusion.

perturbative QCD,

$$\sigma_{hard,res}(s, p_\perp^{cutoff}) = \int dx_1 \int dx_2 \int d\hat{t} \sum_{i,j,k,l} \frac{1}{1+\delta_{k,l}} f_{\gamma,i}(x_1, Q^2) f_{p,j}(x_2, Q^2) \frac{d\sigma^{QCD}_{i,j\to k,l}(\hat{s}, \hat{t})}{d\hat{t}}, \tag{2}$$

where $f_{\gamma,i}(x_1, Q^2)$ and $f_{p,i}(x_2, Q^2)$ denote the parton distribution functions of the photon and proton for the parton i. The sum runs over all possible parton configurations i, j, k, l. For example, we show in figure 2 a gluon-gluon scattering subprocess.

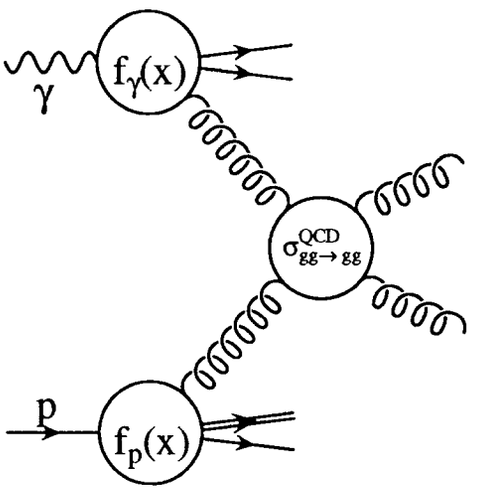

Figure 2: Hard process contributing to resolved γp scattering.

In our approach, all the graphs of lowest order perturbative QCD form the *hard* part of the Pomeron. We assume that the remaining hadronic part can be described by a parametrization frequently used for the so called *soft* Pomeron. In contrast to [7, 9] we use a supercritical *soft* Pomeron as demanded by our fits to the cross sections [25, 26].

This splitting of the Pomeron into *hard* and *soft* Pomerons is totally artificial but enables us to use well confirmed results of the Parton model.

In addition to the Pomeron pole with $\alpha_P(0) \approx 1$ we have to include at least one effective Reggeon pole with $\alpha_R(0) \approx 0.5$ at center of mass energies $\sqrt{s}$ in the region of 5 to 10 GeV.

The general single Reggeon amplitude can be written as

$$A(s,t) = g^0_{P,p}\, g^0_{P,q\bar{q}}\, \eta(\alpha(0)) \left(\frac{s}{s_0}\right)^{\alpha(0)} \exp(\lambda(s)\, t) \quad \text{with} \quad \lambda(s) = b^0 + \alpha'(0) \left(\ln\left(\frac{s}{s_0}\right) - i\frac{\pi}{2}\right) \tag{3}$$

where $g^0_{P,p}$ and $g^0_{P,q\bar{q}}$ denote the momentum transfer independent part of the Reggeon-proton and Reggeon-$q\bar{q}$ state coupling constant. The corresponding Reggeon trajectory and signature factor are

$$\alpha(t) = \alpha(0) + \alpha'(0)t \quad \text{and} \quad \eta(\alpha(t)) = -\left\{1 + \sigma \exp(-i\pi\alpha(t))\right\} / \sin \pi\alpha(t) \tag{4}$$

where $\sigma = \pm 1$ denotes the signature of the Reggeon pole. The parameter $b^0 = \frac{1}{2}b^0_p + \frac{1}{2}b^0_{q\bar{q}}$ results from the coupling constants

$$g_{P,p}(t) = g^0_{P,p}\, \exp(\frac{1}{2}b^0_p\, t) \quad \text{and} \quad g_{P,q\bar{q}}(t) = g^0_{P,q\bar{q}}\, \exp(\frac{1}{2}b^0_{q\bar{q}}\, t). \tag{5}$$

In the following the real part of the Reggeon amplitude will be neglected. This approximation is justified by the restriction to high-energy photoproduction.

The splitting of the resolved processes into hard and soft contributions depends crucially on the value of the $p_\perp^{cutoff}$ parameter but, due to the unitarization, the dependence of the physical cross sections on this parameter is strongly reduced.

3 The eikonal approximation and diffraction

At high energies absorptive corrections to the single Pomeron amplitude Eq. (3) cannot be neglected. Therefore, we use an eikonal approximation to estimate the hadronic amplitude of photon proton interactions. The contribution to the amplitude resulting from direct processes can be treated separately since the direct cross section is small in comparison to the resolved cross section. Hence we unitarize the resolved hard and soft contributions only.

The calculation of the absorptive corrections in the framework of Gribov's Reggeon calculus[27, 28] and the assumption that the multiple discontinuity (see Fig. 3)

$$N^{(n)}_a(\vec{q}_i) = \int \frac{dM^2_{a,1}}{\pi} \cdots \frac{dM^2_{a,(n-1)}}{\pi} Disc_{M^2_{a,1}\ldots M^2_{a,(n-1)}} T^{(n)}_a(\vec{q}_i, M^2_{a,1}, \ldots, M^2_{a,(n-1)}) \tag{6}$$

can be approximated by the product of pole contributions (i.e. coupling constants)

$$N^{(n)}_a(\vec{q}_i) \approx \prod_{k=1}^{n} g_{P,a}(\vec{q}_k) \tag{7}$$

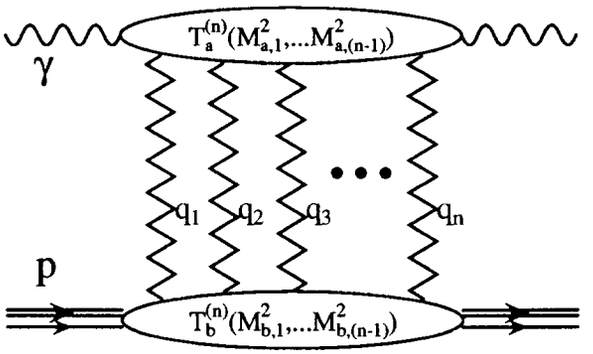

Figure 3: Graph with n Pomeron exchange contributing to the eikonal approximation.

lead to the standard eikonal approximation (see for example [29] and references therein). Here the masses of the intermediate states are labeled by $M_{a,1}$, $M_{a,2}$, ..., $M_{a,(n-1)}$. But in this case the unitarity cuts not passing through any Pomeron involve only elastic intermediate states rather than diffractive and elastic states.

It is known from hadron hadron collider experiments that the total diffractive cross section at high energies becomes comparable to the elastic cross section. Therefore, the inelastic absorptive corrections cannot be neglected. The main contribution to these corrections results from diffractive intermediate states with low masses. For definiteness consider the diffractive contribution resulting from the two Pomeron exchange graph shown in Fig. 4. We subdivide the unitarity sum running over all possible intermediate

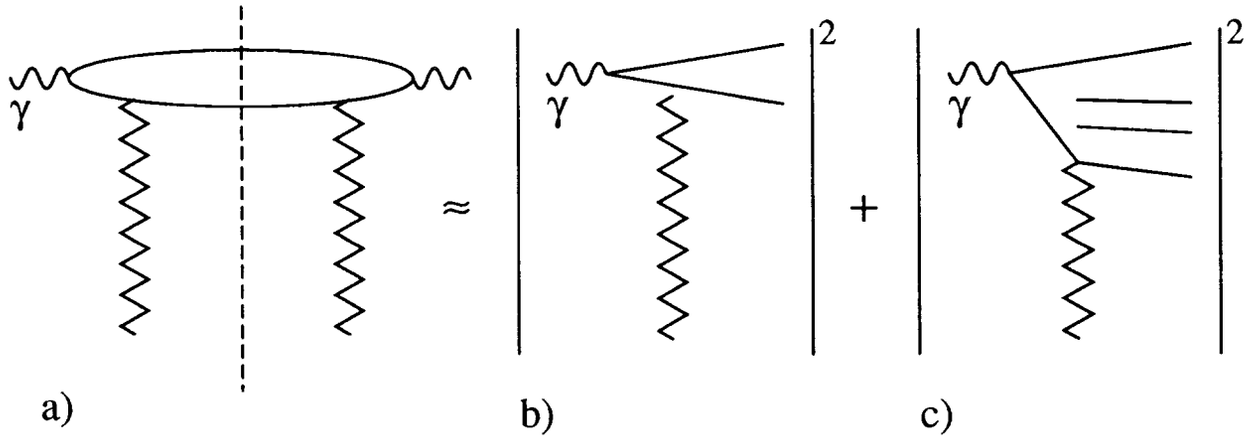

Figure 4: Approximation of the diffractive contribution of the two Pomeron graph: a) Two Pomeron graph with diffractive cut, b) low mass and elastic states, and c) multiperipheral high mass states.

states into elastic, low mass and high mass states. In the following diffractively produced particle systems with a mass lower than $\Sigma_L = 5\text{GeV}^2$ are called low mass excitations. In the case of the photon as incoming particle we consider the quasi-elastically produced ρ^0, ω and ϕ mesons as elastic states.

Assuming multiperipheral kinematics we can use Regge theory to calculate the amplitudes for the elastic and high mass intermediate states. The low mass states can be treated by summing all possible resonances up to a certain mass scale. This would, however, result

in a model with too many free parameters. In order to get an efficient approximation, it is reasonable to introduce a generic low mass resonance as done in Ref. [30]. The amplitude characterizing the transition from the particle to this resonance and via versa cannot be calculated without further assumptions. We will comment on this later.

The contributions of higher diffractive masses $M_D^2 > \Sigma_L$ to the diffractive cut can be calculated using the triple and loop Pomeron graphs (see Fig. 5) [31, 30]. To maintain

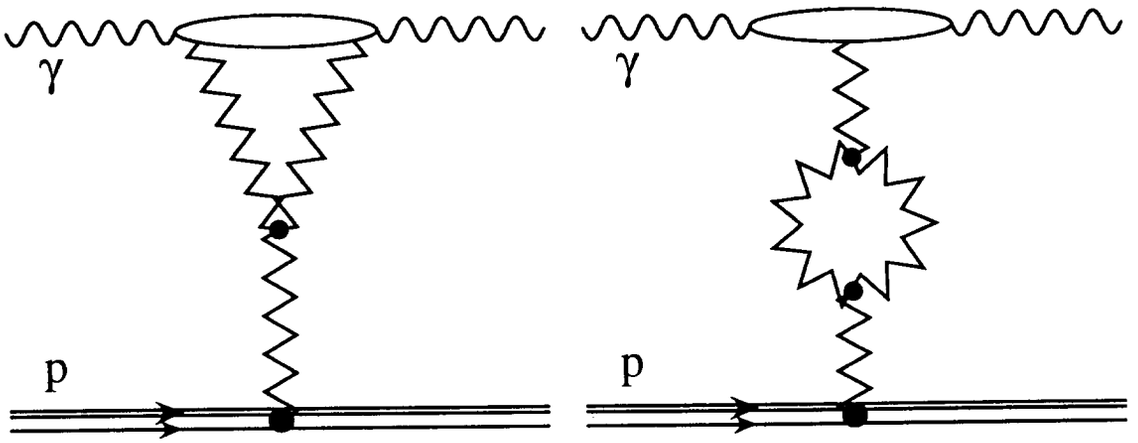

Figure 5: Simplest enhanced graphs: a) triple Pomeron graph, b) loop Pomeron graph

consistency we have to make sure that the terms in the scattering amplitude containing multiple triple or loop Pomeron graphs are small in comparison to the lowest order graphs. This is guaranteed by the smallness of the triple Pomeron coupling g_{3P} and the restriction to energies $\sqrt{s}$ below 500 GeV [32]. At higher energies it is necessary to include further graphs in the unitarization. Using a reasonable ansatz for the multi-Pomeron coupling, the summation of these graphs can be done [33]. Note that the triple and loop Pomeron amplitudes have opposite sign to the single Pomeron amplitude. This is a manifestation of the absorptive character of diffraction.

Now we discuss a simple ansatz for the amplitude describing the transition to a low mass excitation. For simplicity it is assumed that the dynamics of this process can be described by an amplitude similar to the elastic amplitude Eq. (3) but with mass dependent coupling constants and slopes.

One requirement is that there should be a smooth transition between the low mass and the high mass amplitude given by the triple or loop Pomeron graph. The mass dependent slope of the single Pomeron amplitude Eq. (3) can be parametrized by (see Fig. 6)

$$b_P(M_1^2, M_2^2, M_3^2, M_4^2) = b_P^0(M_1^2, M_2^2, M_3^2, M_4^2) + \alpha'(0) \ln \frac{ss_0}{(M_1^2 + M_3^2)(M_2^2 + M_4^2)}. \qquad (8)$$

For $b_P^0(M_1^2, M_2^2, M_3^2, M_4^2)$ we make the following ansatz

$$b_P^0(M_1^2, M_2^2, M_3^2, M_4^2) = \tilde{b}_{P,q\bar{q}}^0 \, e^{-c\,(M_1 - M_3)^2} + \tilde{b}_{P,p}^0 \, e^{-c\,(M_2 - M_4)^2}. \qquad (9)$$

Here $\tilde{b}_{P,p}^0$ and $\tilde{b}_{P,q\bar{q}}^0$ are energy and mass independent parameters and $c = 3\mathrm{GeV}^{-2}$. In the limit of high masses M_3 and M_4, this ansatz reproduces the correct diffractive slopes b_{SD}

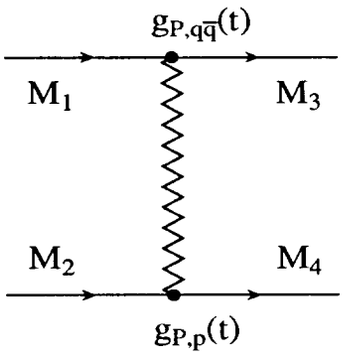

Figure 6: Interaction of particles or resonances by Pomeron exchange

and b_{DD} for single and double diffraction, respectively:

$$\begin{aligned} 2b_P(s, M_1^2, M_2^2, M_3^2, M_4^2) &\overset{s\gg M_3^2\gg M_1^2}{\longrightarrow} & b_{SD} &\approx b_P^0 + 2\alpha'(0)\ln\frac{s}{M_3^2}; \\ 2b_P(s, M_1^2, M_2^2, M_3^2, M_4^2) &\overset{s\gg M_3^2, M_4^2\gg M_1^2, M_2^2}{\longrightarrow} & b_{DD} &\approx 2\alpha'(0)\ln\frac{ss_0}{M_3^2 M_4^2} \end{aligned} \quad . \tag{10}$$

Here we have assumed that the slope parameter b_{3P} of the triple Pomeron coupling,

$$g_{3P}(\vec{q}_1, \vec{q}_2, \vec{q}_3) = g_{3P}^0 \ \exp\left\{b_{3P}\frac{1}{2}(\vec{q}_1^{\,2} + \vec{q}_2^{\,2} + \vec{q}_3^{\,2})\right\} \tag{11}$$

can be neglected in comparison to b_P^0. In Fig. 7 we show the slope Eq. (8) together with data for pions and photons incident on protons at $\sqrt{s} \approx 15$ GeV [34, 35]. The same slope behaviour can be assumed for the proton diffractive vertex as shown in Fig. 8. The data on proton diffraction and elastic scattering are taken from [36] and [37].

The low mass distribution in diffractive processes is connected to the appropriate high mass distribution by finite mass sum rules (FMSRs) [38, 39]. Diffractive mass distributions have been measured and compared to the first moment FMSR by several experimental groups (see for example [40, 41, 35]). Within the experimental uncertainties, no violation of the FMSRs was found. The first moment FMSR can be written as

$$|t|\left(\frac{d\sigma_{el}}{dt}\right)_{exper} + \int_{\nu_{st}}^{\nu_{cut}} \nu \left(\frac{d\sigma_{SD}}{dt\, d\nu}\right)_{exper} d\nu = \int_{\nu_{st}}^{\nu_{cut}} \nu \left(\frac{d\sigma_{SD}}{dt\, d\nu}\right)_{param} d\nu \tag{12}$$

where ν and M_{SD} denote the cross-symmetric variable $\nu = M_{SD}^2 - M_1^2 - t$ and the diffractively produced mass, respectively. The integral of the RHS in Eq. (12) is taken over a parametrization obtained from high mass single diffraction whereas experimentally measured cross section enter the LHS directly. Using the single Pomeron and triple Pomeron amplitude of the model, the mass dependence of the coupling constants $g_{P,p}^0(M_2^2, M_4^2)$ and $g_{P,q\bar{q}}^0(M_1^2, M_3^2)$ can be estimated (see Fig. 6). Here we assume that multiple scattering processes do not drastically change the relative ratios of the different cross sections of Eq. (12) at energies below $\sqrt{s} \approx 50$ GeV. In this energy range the contribution of the hard Pomeron can be neglected. The lower cutoff of the integral in Eq. (12) is given by the smallest diffractive mass possible, $M_{2\pi}$, and t. The upper cutoff has to be greater

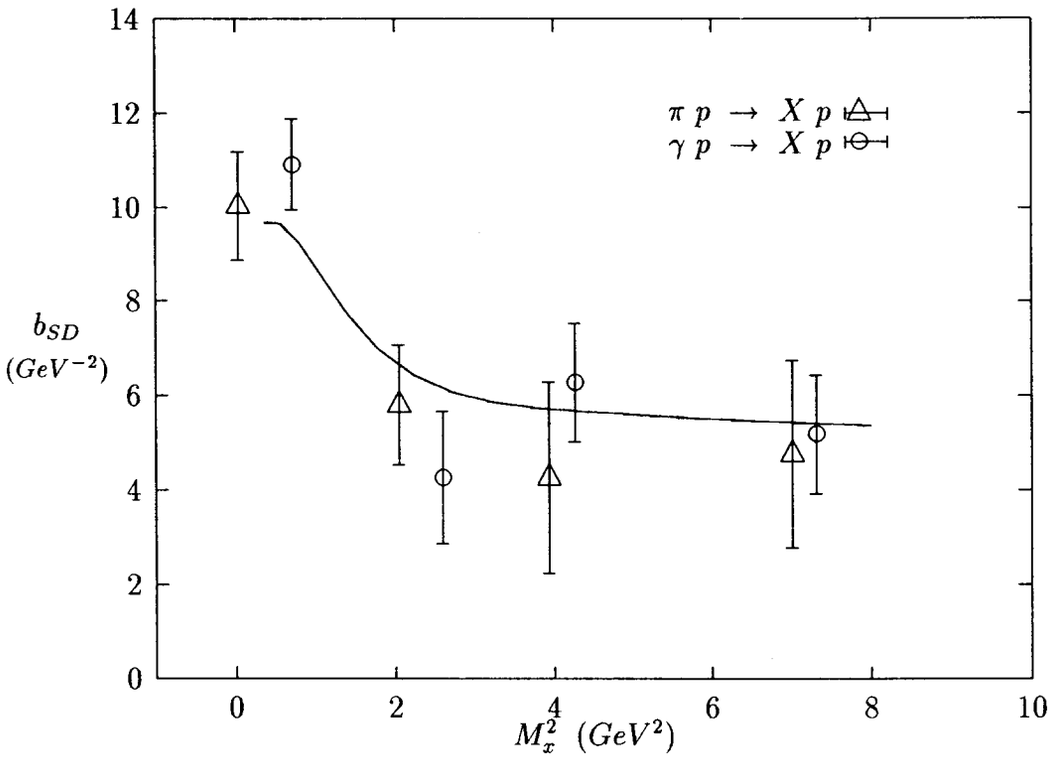

Figure 7: Single diffractive slope b_{SD} in the region 0.02 $(\mathrm{GeV/c})^2 < |t| < 0.1$ $(\mathrm{GeV/c})^2$ as a function of the diffractive mass M_x^2 for $\pi^- p \rightarrow Xp$ and $\gamma p \rightarrow Xp$. The data are taken from [35].

than typical resonance masses. Within the model the upper cutoff coincides with Σ_L. The partial cross sections resulting from the Born amplitudes are:

$$\frac{d\sigma_{el}}{dt} = \frac{1}{16\pi} g_{P,q\bar{q}}^2(0) g_{P,p}^2(0) \left(\frac{s}{s_0}\right)^{2\Delta_P} \exp\left\{2b_P(M_{\rho^0}^2, M_p^2, M_{\rho^0}^2, M_p^2)\; t\right\}; \quad (13)$$

$$\frac{d\sigma_{SD}^{lm}}{dt\, dM_{SD}^2} = \frac{1}{16\pi} g_{P,q\bar{q}}^2(0) g_{P,p}^2(0) \lambda^2(M_{\rho^0}^2, M_{SD}^2) \left(\frac{s}{s_0}\right)^{2\Delta_P} \times \exp\left\{2b_P(M_{\rho^0}^2, M_p^2, M_{SD}^2, M_p^2)\; t\right\} \delta(M_{SD}^2 - M_R^2); \quad (14)$$

$$\frac{d\sigma_{SD}^{hm}}{dt\, dM_{SD}^2} = \frac{1}{16\pi} g_{P,q\bar{q}}(0) g_{3P}(0) g_{P,p}^2(0) \left(\frac{s}{s_0}\right)^{2\Delta_P} \left(\frac{s_0}{\nu}\right)^{\alpha_P(0)} \times \exp\left\{2b_P(M_{\rho^0}^2, M_p^2, M_{SD}^2, M_p^2)\; t\right\}, \quad (15)$$

with $\Delta_P = \alpha_P(0) - 1$. The slope parameters $b_P(M_1^2, M_2^2, M_3^2, M_4^2)$ are given by Eq. (8). In Eq. (14) the ratio of the elastic coupling to the coupling describing low mass excitation and the mass of the effective low mass resonance are denoted by $\lambda(M_1^2, M_3^2)$ and M_R, respectively. Inserting Eq. (13-15) into Eq. (12) one gets

$$\lambda^2(M_{\rho^0}^2, M_R^2) = \frac{1}{M_R^2 - M_{\rho^0}^2 - t} \left\{ \frac{s_0^2\, g_{3P}(0)}{g_{P,q\bar{q}}(0)\,(1-\Delta)} \exp\left\{\tilde{b}_{P,q\bar{q}}^0 \exp(-c(M_R^2 - M_{\rho^0}^2))\,|t|\right\} \times \left[\left(\frac{\Sigma_L - M_{\rho^0}^2 - t}{s_0}\right)^{1-\Delta} - \left(\frac{M_{2\pi}^2 - M_{\rho^0}^2 - t}{s_0}\right)^{1-\Delta} \right]$$

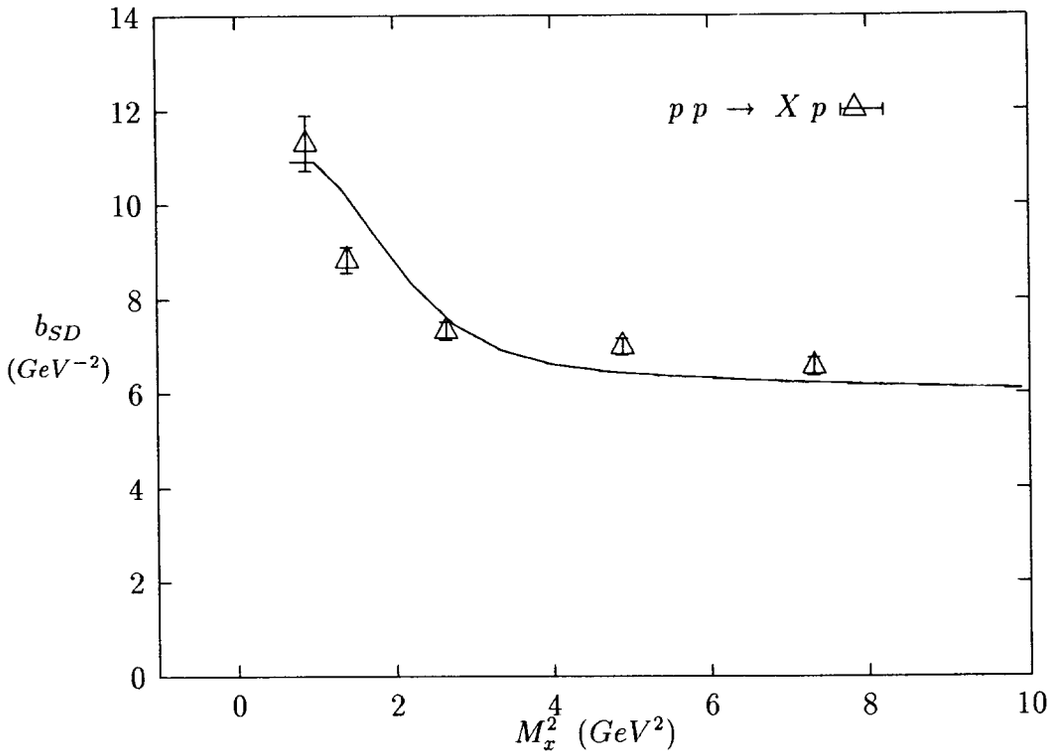

Figure 8: Single diffractive slope b_{SD} in the region 0.15 $(\mathrm{GeV/c})^2 < |t| < 1.45$ $(\mathrm{GeV/c})^2$ as a function of the diffractive mass M_x^2 for $pp \rightarrow Xp$ at ISR [36, 37].

$$-|t| \exp\left\{(\tilde{b}^0_{P,q\bar{q}} \exp(-c(M_R^2 - M_{\rho^0}^2)) - \tilde{b}^0_{P,q\bar{q}} - \tilde{b}^0_{P,p})\,|t|\right\}\Big\} \quad (16)$$

Using the values for the coupling constants explained in Sec. 5 this yields values for λ between 0.3 and 0.5 with t = -0.01 GeV^2. Here we have used the effective resonance masses $M_{R,p}$=1.2GeV and $M_{R,\gamma}$=1GeV for the proton and photon vertices. Taking the triple Pomeron cross section Eq. (15) as high mass parametrization, we have assumed that the triple Pomeron is dual to the diffractive low mass resonances. To account for the other triple Reggeon-Pomeron graphs possible, the value of $\lambda(M_1^2, M_3^2)$ has to be increased by 10-20%.

4 Construction of an effective photoproduction amplitude

In the following we denote the effective low mass resonance states of the proton and $|q\bar{q}\rangle$ by $|p^\star\rangle$ and $|q\bar{q}^\star\rangle$, respectively. The coupling constants and momentum transfer independent parts of the slopes are given by the parametrizations Eq. (8) and (16). The masses $M_{p^\star}$ and $M_{q\bar{q}^\star}$ of these resonance states are limited by the masses of the proton or lowest vector meson and the Σ_L parameter of the triple and loop Pomeron graph integrations.

The *hadronic* part of the photon state is built up by superposition of the $|q\bar{q}\rangle$ and $|q\bar{q}^\star\rangle$ states whereas the proton corresponds directly to the $|p\rangle$ state. One gets for the physical

photon

$$|\gamma\rangle = \sqrt{Z_3}\,|\gamma_{bare}\rangle + \frac{e}{f_{q\bar{q}}}\,|q\bar{q}\rangle + \frac{e}{f_{q\bar{q}^\star}}\,|q\bar{q}^\star\rangle \tag{17}$$

with

$$Z_3 = 1 - e\,\sqrt{\frac{1}{f_{q\bar{q}}^2} + \frac{1}{f_{q\bar{q}^\star}^2}}, \tag{18}$$

where e denotes the elementary charge.

The absorptive corrections to the direct processes are suppressed by the factor e^2/f^2 and can be neglected. Therefore, we unitarize only the resolved Born amplitude by eikonalization. Using the transformation into the impact parameter space

$$a_{(i)}(\vec{B},s) = \frac{-i}{4s}\int \frac{d^2\vec{q}_\perp}{2\pi} A^{(i)}(s,t)e^{-i\vec{q}_\perp\cdot\vec{B}} \qquad i = P,R,H,TP,L \tag{19}$$

one can define the mass dependent Born amplitude of the resolved processes by

$$\begin{aligned} a_B(M_1^2,M_2^2,M_3^2,M_4^2) &= a_P(M_1^2,M_2^2,M_3^2,M_4^2) + a_R(M_1^2,M_2^2,M_3^2,M_4^2) + \\ & a_H(M_1^2,M_2^2,M_3^2,M_4^2) + a_{TP}(M_1^2,M_2^2,M_3^2,M_4^2) + a_L(M_1^2,M_2^2,M_3^2,M_4^2) \end{aligned} \tag{20}$$

where the subscripts P, R, H, TP, and L are used to denote the soft Pomeron, Reggeon, hard Pomeron, triple Pomeron, and loop Pomeron amplitudes. For simplicity we have omitted the arguments s and $\vec{B}$. The complete impact parameter expressions for the Born amplitudes are given in appendix A.

In order to sum all eikonal graphs involving different configurations of particles or resonances we write the eikonal function $\chi(s,\vec{B})$ as the matrix

$$\chi(s,\vec{B}) =$$

$$\begin{pmatrix} a_B(q\bar{q},p\to q\bar{q},p) & a_B(q\bar{q}^\star,p\to q\bar{q},p) & a_B(q\bar{q},p^\star\to q\bar{q},p) & a_B(q\bar{q}^\star,p^\star\to q\bar{q},p) \\ a_B(q\bar{q},p\to q\bar{q}^\star,p) & a_B(q\bar{q}^\star,p\to q\bar{q}^\star,p) & a_B(q\bar{q},p^\star\to q\bar{q}^\star,p) & a_B(q\bar{q}^\star,p^\star\to q\bar{q}^\star,p) \\ a_B(q\bar{q},p\to q\bar{q},p^\star) & a_B(q\bar{q}^\star,p\to q\bar{q},p^\star) & a_B(q\bar{q},p^\star\to q\bar{q},p^\star) & a_B(q\bar{q}^\star,p^\star\to q\bar{q},p^\star) \\ a_B(q\bar{q},p\to q\bar{q}^\star,p^\star) & a_B(q\bar{q}^\star,p\to q\bar{q}^\star,p^\star) & a_B(q\bar{q},p^\star\to q\bar{q}^\star,p^\star) & a_B(q\bar{q}^\star,p^\star\to q\bar{q}^\star,p^\star) \end{pmatrix} \tag{21}$$

Due to unitarity the eigenvalues of the matrix $\chi(s,\vec{B})$ have to be non-negative for all impact parameters $\vec{B}$. This can be expressed approximately by the inequalities:

$$\frac{a_B(s,\vec{B}=0;q\bar{q},p\to q\bar{q},p)}{b(q\bar{q},p\to q\bar{q},p)} \geq \frac{a_B(s,\vec{B}=0;q\bar{q},p\to q\bar{q}^\star,p)}{b(q\bar{q},p\to q\bar{q}^\star,p)} \tag{22}$$

$$\frac{a_B(s,\vec{B}=0;q\bar{q},p\to q\bar{q},p)}{b(q\bar{q},p\to q\bar{q},p)} \geq \frac{a_B(s,\vec{B}=0;q\bar{q},p\to q\bar{q},p^\star)}{b(q\bar{q},p\to q\bar{q},p^\star)} \tag{23}$$

$$\frac{a_B(s,\vec{B}=0;q\bar{q},p\to q\bar{q},p)}{b(q\bar{q},p\to q\bar{q},p)} \geq \frac{a_B(s,\vec{B}=0;q\bar{q},p\to q\bar{q}^\star,p^\star)}{b(q\bar{q},p\to q\bar{q}^\star,p^\star)}, \tag{24}$$

where the impact parameter amplitude is approximated by

$$a_B(s,\vec{B},\ldots) \approx \frac{a(s,\vec{B}=0,\ldots)}{8\pi b(\ldots)} \exp\left\{-\frac{\vec{B}^2}{4b(\ldots)}\right\}. \tag{25}$$

The effective eikonal amplitude of resolved processes reads

$$a_{res}(s,B) = \frac{i}{2}(1-e^{-\chi(s,B)}). \tag{26}$$

The different amplitudes can be calculated using the states

$$|q\bar{q},p\rangle \simeq \begin{pmatrix}1\\0\\0\\0\end{pmatrix} \qquad |q\bar{q}^\star,p\rangle \simeq \begin{pmatrix}0\\1\\0\\0\end{pmatrix} \qquad |q\bar{q},p^\star\rangle \simeq \begin{pmatrix}0\\0\\1\\0\end{pmatrix}$$
$$|q\bar{q}^\star,p^\star\rangle \simeq \begin{pmatrix}0\\0\\0\\1\end{pmatrix} \qquad |\gamma_{had},p\rangle \simeq \begin{pmatrix}e/f_{q\bar{q}}\\e/f_{q\bar{q}^\star}\\0\\0\end{pmatrix}. \tag{27}$$

With the normalization of Eq. (26), the cross sections are given by:

$$\sigma_{tot} = 4\int d^2B\ \Im m\ (Z_3\ a_{dir}(s,B) + \langle\gamma_{had},p|\ a_{res}(s,B)\ |\gamma_{had},p\rangle) \tag{28}$$
$$\sigma_{el} = 4\int d^2B\ |\ Z_3\ a_{dir}(s,B) + \langle\gamma_{had},p|\ a_{res}(s,B)\ |\gamma_{had},p\rangle\ |^2 \tag{29}$$

where the impact parameter amplitude $a_{dir}(s,B)$ is given in appendix A. The $|q\bar{q}\rangle$ state is essentially a superposition of the low mass vector mesons ρ^0 and ω. Therefore, we can write the cross section of quasi-elastic vector meson production as

$$\sigma_{q-el,\rho^0,\omega} = 4\int d^2B\ |\ \langle q\bar{q},p|\ a_{res}(s,B)\ |\gamma,p\rangle\ |^2. \tag{30}$$

According to the assumptions of the previous section the cross sections for single and double low mass diffractive dissociation are given by:

$$\sigma^{lm}_{SD,p} = 4\int d^2B\ |\ \langle q\bar{q},p^\star|\ a_{res}(s,B)\ |\gamma_{had},p\rangle\ |^2 \tag{31}$$
$$\sigma^{lm}_{SD,\gamma} = 4\int d^2B\ |\ \langle(q\bar{q})_{sd},p|\ a_{res}(s,B)\ |\gamma_{had},p\rangle\ |^2 \tag{32}$$
$$\sigma^{lm}_{DD} = 4\int d^2B\ |\ \langle q\bar{q}^\star,p^\star|\ a_{res}(s,B)\ |\gamma_{had},p\rangle\ |^2. \tag{33}$$

In Eq. (32), the normalized state $\langle (q\bar{q})_{sd}, p|$ orthogonal to $\langle \gamma_{had}, p|$ is introduced to ensure that there is no mixing of low mass quasi-elastic scattering and low mass single diffractive excitation. The elastic $\gamma p \to \gamma p$ amplitude can be neglected in comparison to the single diffractive amplitude in Eq. (32).

The cross sections for high mass single and double diffraction can be calculated using the Abramovski-Gribov-Kancheli cutting rules[42]. We will comment on this in a forthcoming paper and refer the reader to [43, 20]. With the weight factor -1 for the diffractive cut through a triple or loop Pomeron one obtains in lowest order of the triple Pomeron coupling g_{3P}

$$\sigma^{hm}_{SD,\gamma} = \int d^2B \langle \gamma_{had}, p| \, (-2\chi_{TP,\gamma}(s,B)) e^{-2\chi(s,B)} \, |\gamma_{had}, p\rangle \tag{34}$$

$$\sigma^{hm}_{SD,p} = \int d^2B \langle \gamma_{had}, p| \, (-2\chi_{TP,p}(s,B)) e^{-2\chi(s,B)} \, |\gamma_{had}, p\rangle \tag{35}$$

$$\sigma^{hm}_{DD} = \int d^2B \langle \gamma_{had}, p| \, (-2\chi_{L}(s,B)) e^{-2\chi(s,B)} \, |\gamma_{had}, p\rangle \tag{36}$$

For completeness we give the formula to calculate the slope of quasi-elastic vector meson photoproduction [44]

$$b_{\rho^0,\omega} = \frac{\int d^2B \; B^2 \; \langle q\bar{q}, p| \; a_{res}(s,B) \; |\gamma, p\rangle}{2 \int d^2B \; \langle q\bar{q}, p| \; a_{res}(s,B) \; |\gamma, p\rangle}. \tag{37}$$

The expressions for the cross sections resulting from Eq. (28) - (36) and Eq. (21) are given in appendix B.

5 Describing photoproduction data

The free parameters of the model can be determined by a global fit to high-energy photoproduction data.

For the coupling $f_{q\bar{q}}$ we take the value suggested by low energy data $e^2/f^2_{q\bar{q}} \approx 1/220$. It is expected that only a small part of the hadronic component of the photon results from the $q\bar{q}^\star$ state with higher virtuality. Therefore, this coupling is assumed to be roughly 10 times smaller, $e^2/f^2_{q\bar{q}^\star} \approx 1/2200$.

Hadronic data support the hypothesis that the soft Pomeron and Reggeon couple predominantly to quarks [45]. As a direct consequence of this, the ratio of the coupling constants $g^0_{P,p}$ and $g^0_{P,q\bar{q}}$ can be approximated by

$$\frac{g^0_{P,p}}{g^0_{P,q\bar{q}}} = \frac{3}{2} \tag{38}$$

This is in agreement with the values found in [45]. For the constant parts of the elastic slopes b^0_p and $b^0_{q\bar{q}}$ the relation

$$\frac{\tilde{b}^0_p}{\tilde{b}^0_{q\bar{q}}} = \sqrt{\frac{3}{2}} \tag{39}$$

is assumed. The triple Pomeron coupling is independent of the particular scattering process and can be taken from other fits to pp or $p\bar{p}$ cross sections [30]. We use the values $g_{3P} = 0.08\ \sqrt{\text{mb}}\ \text{GeV}^{-2}$ and $b_{3P} = 0.5\ \text{GeV}^{-2}$. The Reggeon intercept is well determined by fits to the masses of particles with the same quantum numbers and is taken from Ref. [45]. For the parameters $\alpha'_P(0)$ and $\alpha'_R(0)$ we use the known values 0.27 GeV^{-2} and 0.9 GeV^{-2}. Since there are not enough data on diffractive cross sections, the resonance masses $M_{q\bar{q}^\star}$ and $M_{p^\star}$ cannot be determined by a fit. We have used the values $M_{q\bar{q}^\star}$=1GeV and $M_{p^\star}$=1.2GeV.

In order to restrict the calculation of the hard input cross section σ^{QCD} to the region in which perturbative QCD and the Parton model are reliable we choose a transverse momentum cutoff of $p_\perp^{cutoff} = 3$ GeV/c. To show the dependence of our results on this parameter a fit was also performed for a cutoff of 2.5 GeV/c. For lower values of the transverse momentum cutoff, the low x region of the parton distribution functions enters the cross section calculation (see Eq. (2)) and would lead to double counting [46].

Thus we have reduced the free parameters to be determined by a fit to the following: the Pomeron intercept $\alpha_P(0)$; the Pomeron proton and Reggeon proton coupling constants $g^0_{P,p}$; and $g^0_{R,p}$; and the slope parameters $\tilde{b}^0_{P,p}$ and $\tilde{b}^0_{R,p}$. We have used for the fit not only the inelastic photoproduction cross sections [4, 2, 6, 47] but also slope data from quasi-elastic vector meson production [6, 48]. Because of the dependence of the hard input cross sections on the parton distribution function (PDF) parametrization used, separate fits for each set of PDF parametrizations are performed. In table (1) we list the values for some photon [49, 50] and proton [51, 52] parton distribution functions.

Table 1: Model parameters obtained by a global fit to the total inelastic photoproduction cross sections and the forward slopes of quasi-elastic vector meson production.

proton PDF	photon PDF	$g^0_P(\sqrt{mb})$	$g^0_R(\sqrt{mb})$	$\alpha_P(0)$	$\tilde{b}^0_{P,p}(GeV^{-2})$	$\tilde{b}^0_{R,p}(GeV^{-2})$
MRS[D0]	GRV 1	4.68	7.80	1.067	3.48	1.63
MRS[D0]	GS 1	4.65	7.88	1.070	3.49	1.63
MRS[D-]	GRV 1	4.69	7.79	1.067	3.48	1.64
CTEQ1L	GS 1	4.63	7.94	1.072	3.48	1.64
CTEQ1MS	GS 1	4.66	7.86	1.070	3.49	1.65

The model allows a good fit to available data on the total photoproduction cross section and to the quasi-elastic vector meson production cross section and slope. In Fig. 9 we compare the inelastic photoproduction cross section with data [4, 2, 53, 54, 47]. In contrast to the fast increasing hard input cross sections the model shows a rather weak energy dependence of the inelastic cross section. This is a result of both the unitarization of the Born amplitudes and the inclusion of inelastic absorptive corrections in the eikonal approximation.

In Fig. 10 we show the diffractive cross sections predicted by the model. As a direct consequence of Eq. (38) and (39) the model predicts a larger single diffractive cross section for the photon vertex in comparison to the proton vertex. Due to the contribution of the

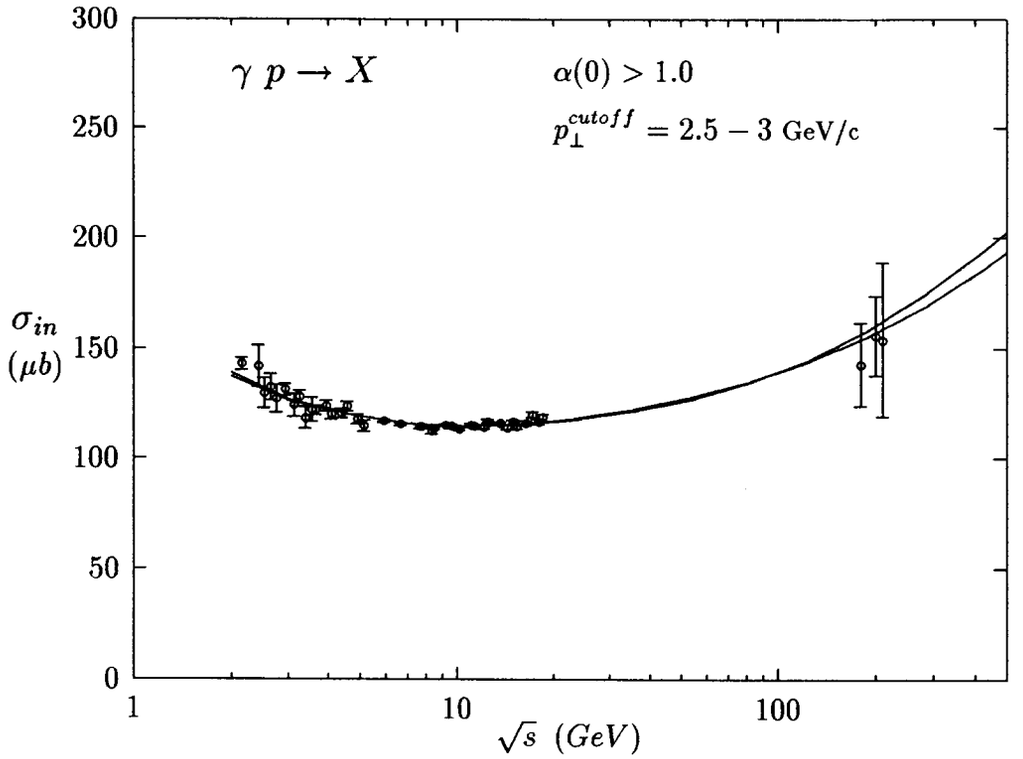

Figure 9: Inelastic $\gamma p \rightarrow X$ cross section as a function of the center of mass energy $\sqrt{s}$ calculated with the model and compared to experimental data. The lower and upper curves correspond to model predictions calculated with a $p_\perp^{cutoff}$ of 2.5 GeV/c and 3 GeV/c, respectively.

triple Pomeron graph to single diffraction the difference between these two cross sections increases with the energy.

In Fig. 11 we compare the cross section of quasi-elastic photoproduction of ρ^0 on protons predicted by the model with data [55]. The high energy measurement is obtained by scaling the total vector meson cross section by 0.82 [53]. In addition, in Fig. 12 the slope of the forward quasi-elastic ρ^0 production calculated with the model and data [48, 6] are shown.

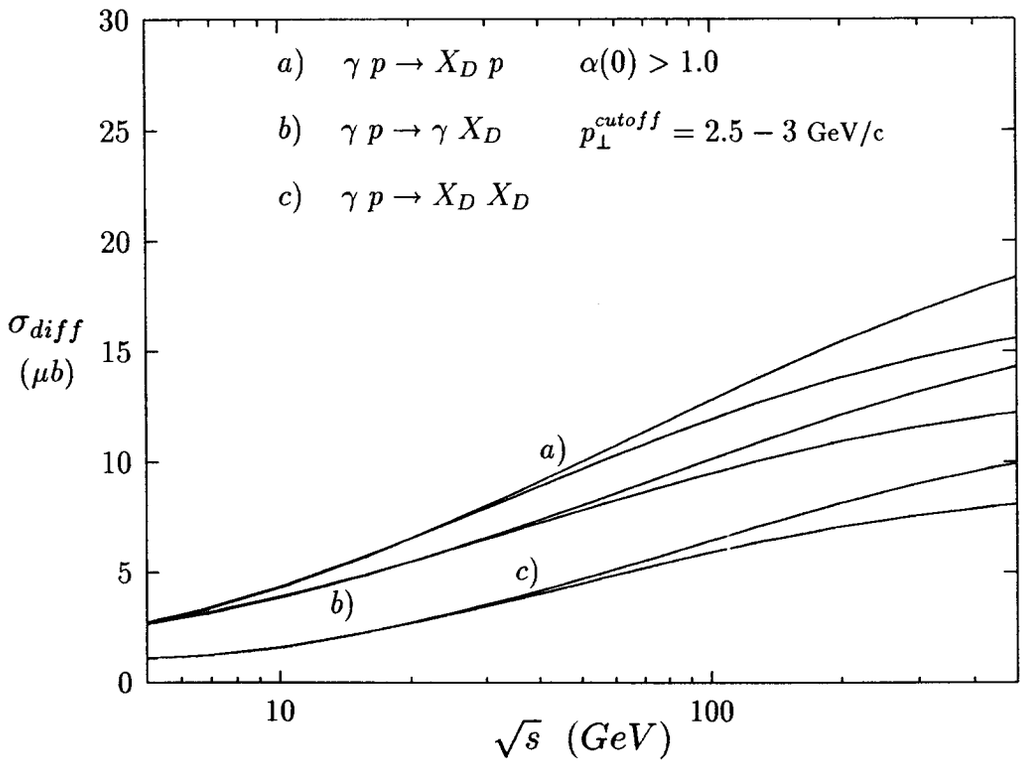

Figure 10: Inelastic diffractive cross sections a) $\gamma p \rightarrow X_D p$, b) $\gamma p \rightarrow \gamma X_D$, and c) $\gamma p \rightarrow X_D X_D$ as a function of the center of mass energy $\sqrt{s}$ calculated with the model. The lower and upper curves correspond to model predictions calculated with a $p_\perp^{cutoff}$ of 2.5 GeV/c and 3 GeV/c, respectively.

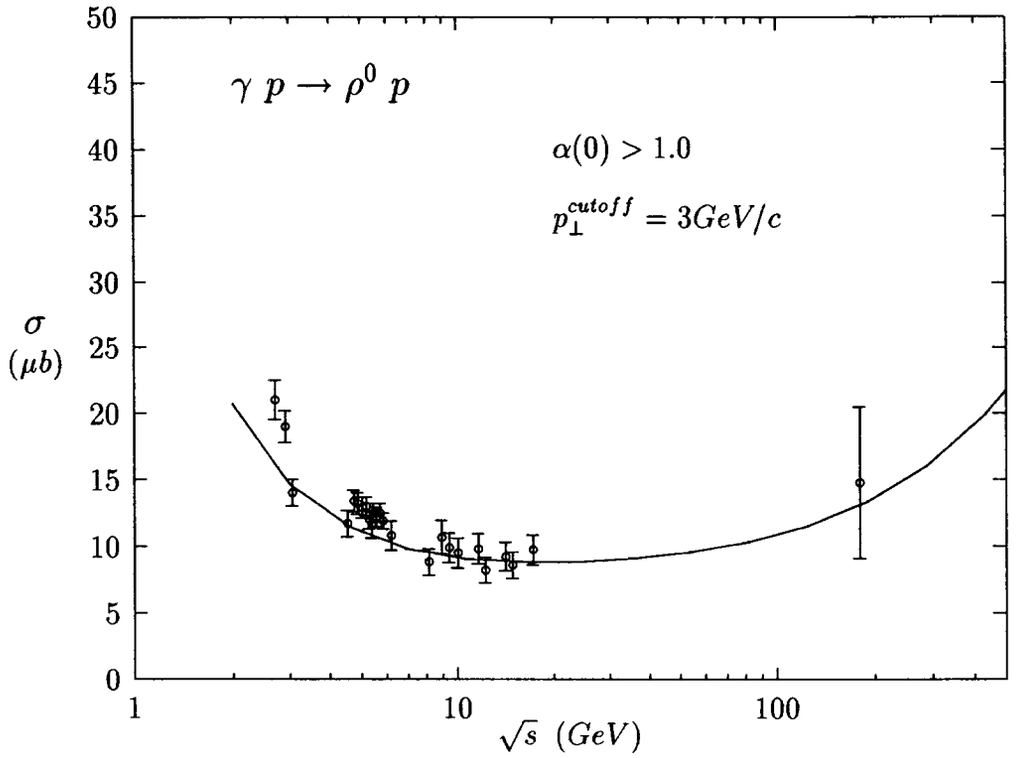

Figure 11: Quasi-elastic $\gamma p \rightarrow \rho^0 p$ cross section as a function of the center of mass energy $\sqrt{s}$ calculated with the model and compared to data [53, 55].

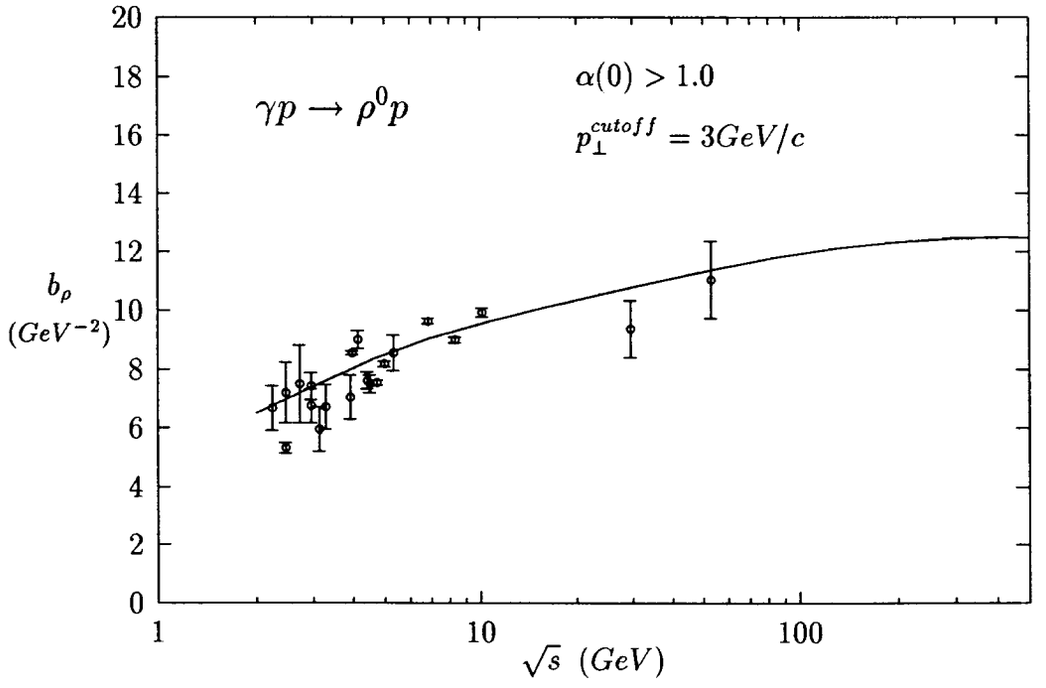

Figure 12: Slope parameter of quasi-elastic ρ^0 production compared with the results calculated with the model. The low energy data are taken from [48], the two high energy measurements are preliminary data of the H1 Collab. [6].

As recently discussed by the authors of [56], the unitarized high mass diffractive amplitude should show a peripheral shape at high energies. Once we have determined the free parameters of the model we can estimate the energy range where the model shows this transition from the central to the peripheral shape. In Fig. 13 we show the unitarized impact parameter amplitude for high mass diffraction Eq. (35). According to the parameters obtained in the fit, the model predicts that the transition to the peripheral shape takes place at energies above $\sqrt{s} = 200$ GeV. Consequently, below this energy the model predicts that the diffractive cross section increases faster than $log(s)$. In Fig. 14 we show the amplitude related to low mass diffraction. Low mass diffraction is approximated in a quite different way (see Eq. (31)) but the resulting amplitude exhibits similar behaviour.

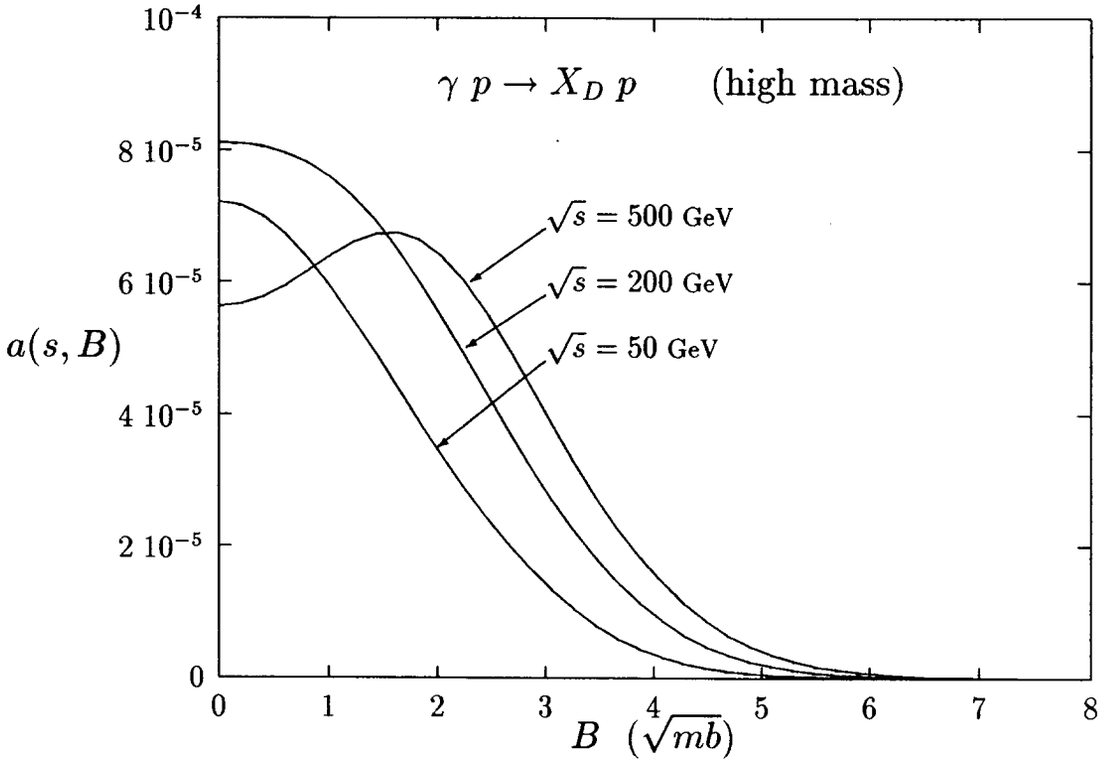

Figure 13: Impact parameter profile of high mass single diffraction (see Eq. (35)) for the collision energies $\sqrt{s} = 50, 200, 500$ GeV.

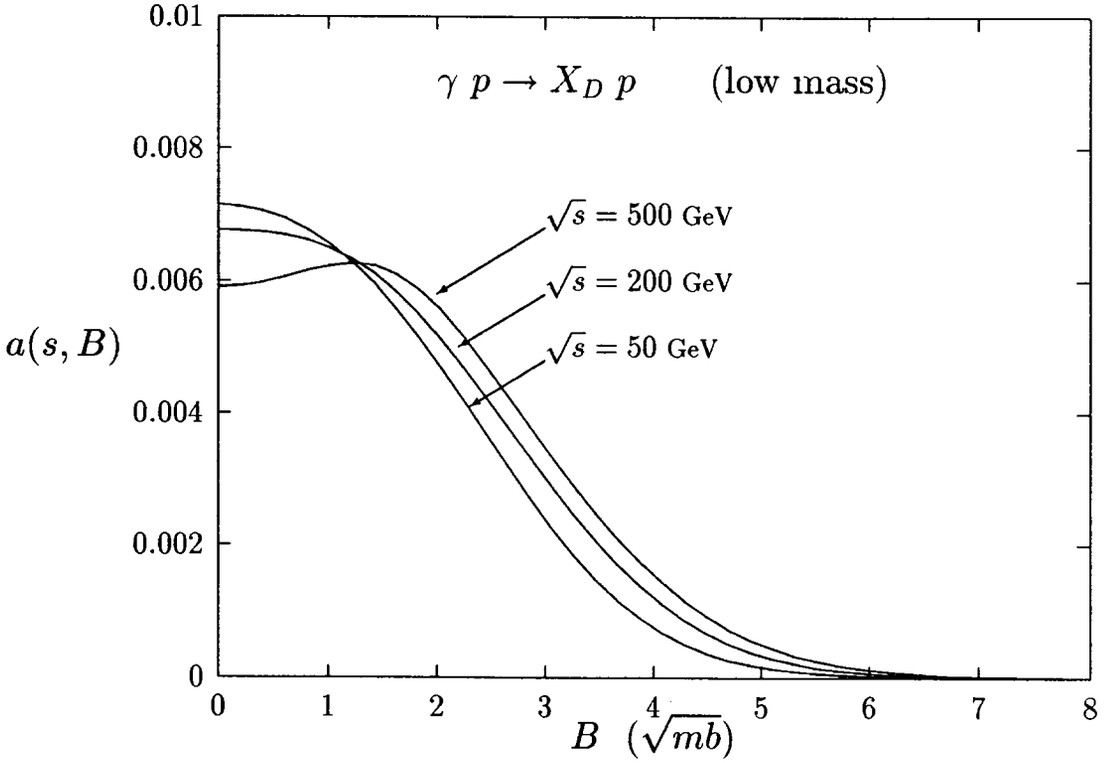

Figure 14: Impact parameter amplitude of low mass single diffraction (see Eq. (31)) for the collision energies $\sqrt{s} = 50, 200, 500$ GeV.

6 Conclusions

A detailed model of photoproduction has been presented, based on the assumptions of the DPM. This allows the construction of soft and hard photoproduction amplitudes. In contrast to [14] we distinguish only two classes of photon hadron interactions, the direct and resolved component rather than the direct, VDM and anomalous component. This obviates the necessity of modifications to the parton distribution functions. Furthermore, this model takes into account elastic and inelastic absorptive corrections by unitarization of the partial cross sections. Introducing a mass dependent slope and parametrization of the coupling constant, we extend the two channel eikonal formalism to get a smooth transition between low and high mass diffraction. High mass inelastic absorptive corrections are treated in lowest order of the triple Pomeron coupling. Within the two channel formalism, both the high mass single diffractive and the low mass single diffractive amplitude show, at high energies, a peripheral impact parameter shape. Using the numerical values resulting from our fits the model predicts that there are no indications for this asymptotic behaviour in the range of HERA energies.

The partial cross sections calculated with the model show an overall agreement with the results obtained in [14], but our model predicts a larger single diffractive cross section of the photon than of the proton. This follows directly from the assumption that the Pomeron couples predominantly to quarks.

Finally we want to emphasize that within the framework of the DPM, the model presented can be used directly for the description of multiparticle photoproduction at high energies [21].

Acknowledgments

We acknowledge valuable discussions with Prof. P. Aurenche, Prof. F.W. Bopp, Prof. A. Capella, Dipl. Phys. I. Kawrakov, Dr. R. Kirschner, and Prof. J. Ranft. We are grateful to Prof. J. Ranft and Dipl. Phys. S. Roesler for useful comments on the manuscript.

This work was supported by the Deutsche Forschungsgemeinschaft under contract number Ra 559/3-1.

References

[1] W. Buchmüller and G. Ingelmann (ed.): Proccedings of the HERA Workshop, Hamburg 1991

[2] T. Ahmed et al.: H1 Collab. Phys. Lett. B299 (1993) 374

[3] I. Abt et al.: H1 Collab. Phys. Lett. B314 (1993) 436

[4] M. Derrick et al.: ZEUS Collab. Phys. Lett. B293 (1992) 465

[5] M. Derrick et al.: ZEUS Collab. Phys. Lett. B322 (1994) 287

[6] G. Knies: J. Phys. G: Nucl. Part. Phys. 19 (1993) 1523

[7] J. Durand and H. Pi: Phys. Rev. Lett. 58 (1987) 2015

[8] J. C. Collins and G. A. Landinsky: Phys. Rev. D43 (1991) 2847

[9] R. Gandhi and I. Sarcevic: Phys. Rev. D44 (1991) 10

[10] R. S. Fletscher, T. K. Gaisser and F. Halzen: Phys. Rev. D45 (1992) 337

[11] R. S. Fletscher, T. K. Gaisser and F. Halzen: (erratum) Phys. Rev. D45 (1992) 3279

[12] J. R. Forshaw and J. K. Storrow: Phys. Rev. D46 (1992) 4955

[13] G. A. Schuler and T. Sjöstrand: Phys. Lett. B300 (1993) 169

[14] G. A. Schuler and T. Sjöstrand: Nucl. Phys. B407 (1993) 539

[15] G. Ingelman: Comput. Phys. Commun. 46 (1987) 217

[16] G. Ingelman and A. Weigend: Comput. Phys. Commun. 46 (1987) 241

[17] G. Marchesini et al.: Comput. Phys. Commun. 67 (1992) 456

[18] J. Butterworth and J. R. Forshaw: J. Phys. G: Nucl. Part. Phys. 19 (1993) 1657

[19] A. Capella, U. Sukhatme, C. I. Tan and J. Tran Thanh Van: Phys. Rep. 236 (1994) 227

[20] P. Aurenche, F. W. Bopp, A. Capella, J. Kwiecinski, M. Maire, J. Ranft and J. Tran Thanh Van: Phys. Rev. D45 (1992) 92

[21] R. Engel: in preparation

[22] J. J. Sakurai: Ann. Phys. 11 (1960) 1

[23] J. J. Sakurai and D. Schildknecht: Phys. Lett. 40B (1972) 121

[24] P. Soeding: Phys. Lett. B19 (1966) 702

[25] R. Engel, F. W. Bopp, D. Pertermann and J. Ranft: Phys. Rev. D46 (1992) 5192

[26] F. W. Bopp, D. Pertermann, R. Engel and Ranft: Phys. Rev. D49 (1994) 3228

[27] V. N. Gribov: Zh. Eksp. Teor. Fiz. 26 (1968) 414

[28] V. N. Gribov: Zh. Eksp. Teor. Fiz. 26 (1969) 1306

[29] A. B. Kaidalov: Phys. Rep. 50 (1979) 157

[30] A. Capella, J. Tran Thanh Van and J. Kaplan: Nucl. Phys. B97 (1975) 493

[31] A. Capella and J. Kaplan: Phys. Lett. 52B (1974) 448

[32] C. Pajares, A. Varias and P. Yepes: Z. Phys. C–Particles and Fields 19 (1983) 89

[33] A. B. Kaidalov, L. A. Ponomarev and K. A. Ter-Martirosyan: Yad. Fis. 44 (1986) 722

[34] K. Goulianos: Phys. Rep. 101 (1983) 169

[35] T. J. Chapin et al.: Phys. Rev. D31 (1985) 17

[36] M. G. Albrow et al.: Nucl. Phys. B108 (1976) 1

[37] A. Breakstone et al.: ABCDHW Collab Nucl. Phys. B248 (1984) 253

[38] A. I. Sanda: Phys. Rev. D6 (1972) 280

[39] M. B. Einhorn, J. Ellis and J. Finkelstein: Phys. Rev. D5 (1972) 2063

[40] R. D. Field and G. C. Fox: Nucl. Phys. B80 (1974) 367

[41] D. P. Roy and R. G. Roberts: Nucl. Phys. B77 (1974) 240

[42] V. A. Abramovski, V. N. Gribov and O. V. Kancheli: Yad. Fis. 18 (1973) 595

[43] A. Capella, J. Kaplan and J. Tran Thanh Van: Nucl. Phys. B105 (1976) 333

[44] M. M. Block and R. N. Cahn: Rev. Mod. Phys. 57 (1985) 563

[45] A. Donnachie and P. V. Landshoff: Phys. Lett. B296 (1993) 227

[46] J. Kwiecinski: Phys. Lett. B194 (1987) 386

[47] S. I. Alekhin et al.: Compilation of cross sections 4 CERN-HERA 87-01 1987

[48] D. Aston et al.: Nucl. Phys. B209 (1982) 56 and references therein

[49] M. Glück, E. Reya and A. Vogt: Z. Phys. C–Particles and Fields C53 (1992) 127

[50] M. Drees and K. Grassie: Z. Phys. C–Particles and Fields C28 (1992) 451

[51] A. D. Martin, R. G. Roberts and W. J. Stirling: Phys. Rev. D47 (1993) 867

[52] J. Botts et al.: Phys. Lett. B304 (1993) 159

[53] M. Derrick et al.: ZEUS Collab. DESY Preprint 94-32 1994

[54] D. O. Caldwell: Phys. Rev. Lett. 40 (1978) 1222

[55] H. Schopper (ed.): *Total Cross-Sections for Reactions of High Energy Particles* Landolt-Börnstein, New Series, Vol. 12b 1987

[56] E. Gotsman, E. M. Levin and U. Maor: FERMILAB-PUB-93/000-T 1993

[57] J. Kwiecinski: Z. Phys. C–Particles and Fields C29 (1985) 147

[58] A. Capella, J. Tran Thanh Van and J. Kwiecinski: Phys. Rev. Lett. 58 (1987) 2015

Appendix A

In the following we give the complete expressions for the Born amplitudes transformed into the impact parameter representation.

In the formulae, the dependence on the external masses (see Fig. 6) is symbolized by M_k. All the amplitudes are approximated by a gaussian impact parameter dependence

$$a_{B,i}(s,\vec{B};M_k^2) = \frac{\sigma_{B,i}^{tot}(s;M_k^2)}{8\pi\ b_i(s,M_k^2)} \exp\left\{-\frac{\vec{B}^2}{4\ b_i(s,M_k^2)}\right\}. \tag{40}$$

The index i stands for P, R, H, TP, and L which denote the soft Pomeron, Reggeon, hard Pomeron, triple Pomeron, and loop Pomeron amplitude, respectively.

The Pomeron and Reggeon total cross sections are parametrized by (see Eq. (3))

$$\sigma_{B,P}^{tot}(s) = g_{P,p}^0(M_k^2)\ g_{P,q\bar{q}}^0(M_k^2)\ \left(\frac{s}{s_0}\right)^{\Delta_P} \qquad \sigma_{B,R}^{tot}(s) = g_{R,p}^0(M_k^2)\ g_{R,q\bar{q}}^0(M_k^2)\ \left(\frac{s}{s_0}\right)^{\Delta_R} \tag{41}$$

with $\Delta_P = \alpha_P(0) - 1$ and $\Delta_R = \alpha_R(0) - 1$. The slope parameters $b_P(M_k^2)$ and $b_R(M_k^2)$ are given by the parametrizations Eq. (8) and Eq. (9).

The hard resolved cross section is calculated from Eq. (2) using the scale $Q^2 = p_\perp^2$. The hard input cross section then reads

$$\sigma_{B,H}^{tot} = \sigma_{hard,res}^{QCD}(s, p_\perp^{cutoff}) \left(\frac{e^2}{f_{q\bar{q}}^2} + \frac{e^2}{f_{q\bar{q}^\star}^2}\right)^{-1}. \tag{42}$$

It is assumed that the hard Pomeron contributes to low mass diffraction in a way similar to the soft Pomeron. Therefore, the hard input cross section is scaled by the ratio resulting from the soft Pomeron couplings. The impact parameter amplitude of the hard Pomeron is written as Eq. (40) with $b_H = 1.5\ \mathrm{GeV}^{-2}$. The slope of the hard Pomeron is assumed to be energy independent [57, 58]. The direct input cross section is calculated from Eq. (1) with the same cutoff as used for the resolved hard contribution. The impact parameter amplitude $a_{dir}(s,\vec{B})$ is also approximated by Eq. (40).

The calculation of the input cross section resulting from the triple Pomeron graph shown in Fig. 5 a) yields [31, 30]

$$\begin{aligned}\sigma_{TP,a}(s,q^2=0) = -is_0 \frac{g_b^2(0)\, g_a(0)\, g_{3P}^0}{16\pi\, 2\alpha'(0)} \left(\frac{s}{s_0}\right)^{\Delta_P} \exp\left(-\frac{b_b^0 + b_{3P}}{2\alpha'}\Delta_P\right) \\ \times \left\{E_i\left[\left(\frac{b_b^0 + b_{3P}}{2\alpha'(0)} + \ln\frac{s}{\Sigma_L}\right)\Delta_P\right] - E_i\left[\left(\frac{b_b + b_{3P}}{2\alpha'(0)} + \ln\Sigma_U\right)\Delta_P\right]\right\}\end{aligned} \tag{43}$$

where the integration over the diffractive mass M_D is performed from $M_D^2 = \Sigma_L$ to $M_D^2 = s/\Sigma_U$.

The contribution of the loop Pomeron shown in Fig. 5 b) can be written as [30]

$$\begin{aligned}\sigma_L(s,q^2=0) = -is_0^2 \frac{g_a(0)\, g_b(0)\, (g_{3P}^0)^2}{16\pi\, 2\alpha'(0)} \left(\frac{s}{s_0}\right)^{\Delta_P} \exp\left(-\frac{\Delta_P b_{3P}}{\alpha'}\right) \\ \times \left\{\left(\frac{b_{3P}}{\alpha'(0)} + \ln\frac{ss_0}{\Sigma_L^2}\right)\left\{E_i\left[\left(\frac{b_{3P}}{\alpha'(0)} + \ln\frac{ss_0}{\Sigma_L^2}\right)\Delta_P\right] - E_i\left[\left(\frac{b_{3P}}{\alpha'(0)} + \ln\Sigma_U\right)\Delta_P\right]\right\}\right. \\ \left. + \frac{1}{\Delta_P}\exp\left[\left(\frac{b_{3P}}{\alpha'(0)} + \ln\Sigma_U\right)\Delta_P\right] - \frac{1}{\Delta_P}\exp\left[\left(\frac{b_{3P}}{\alpha'(0)} + \ln\frac{ss_0}{\Sigma_L^2}\right)\Delta_P\right]\right\}\end{aligned} \tag{44}$$

The integrations over the masses $M_{D,1}$ and $M_{D,2}$ are performed from $M_{D,1}^2 = M_{D,2}^2 = \Sigma_L$ to $M_{D,1}^2 M_{D,2}^2 = ss_0/\Sigma_U$. Following Ref. [30] we take $\Sigma_U = 2.5$ and $\Sigma_L = 5$ GeV^2.

For numerical calculations we use an effective exponential t dependence of the triple and loop Pomeron introduced in Ref. [31].

$$A_{TP}^a(s,t) = A_{TP}^a(s,0)\,\exp\left(b_{TP}^a\, t\right) \tag{45}$$

$$A_L(s,t) = A_L(s,0)\,\exp\left(b_L\, t\right) \tag{46}$$

where the slope parameters b_{TP}^a and b_L are given by

$$\begin{aligned} b_{TP}^a &= \frac{1}{2}\left(b_a^0 + b_b^0\right) + b_{3P} + \alpha'(0)\ln\frac{s}{s_0} \\ &- \frac{1}{2}\alpha'(0)\,\ln\frac{s}{\Sigma_L\,\Sigma_U}\left(\ln\frac{b_b^0 + b_{3P} + 2\alpha'(0)\,\ln(s/\Sigma_L)}{b_b^0 + b_{3P} + 2\alpha'(0)\,\ln\Sigma_U}\right)^{-1} \end{aligned} \tag{47}$$

$$\begin{aligned} b_L &= \frac{1}{2}\left(b_a^0 + b_b^0\right) + 2b_{3P} + \alpha'(0)\,\ln\frac{s}{s_0} \\ &- \frac{1}{4}\,\alpha'(0)\,\ln^2\frac{ss_0}{\Sigma_U\,\Sigma_L^2}\left\{\ln\left|\frac{b_{3P}/\alpha'(0) + \ln\frac{ss_0}{\Sigma_L^2}}{b_{3P}/\alpha'(0) + \ln\Sigma_U}\right|\left(\frac{b_{3P}}{\alpha'(0)} + \ln\frac{ss_0}{\Sigma_L^2} - \ln\frac{ss_0}{\Sigma_U\,\Sigma_L^2}\right)\right\}^{-1} \end{aligned} \tag{48}$$

We want to emphasize that b_{TP}^a and b_L are the effective slopes of the uncut graphs shown in Fig. 5 a) and b) and not the diffractive slopes b_{SD} and b_{DD} relevant to the description of single and double diffraction.

Appendix B

The eikonal matrix $\chi(s,B)$ (see Eq. (21)) can be written as the sum of the eikonal matrices related to the different graphs.

$$\chi(s,B) = \chi_P(s,B) + \chi_R(s,B) + \chi_H(s,B) + \chi_{TP,\gamma}(s,B) + \chi_{TP,p}(s,B) + \chi_L(s,B) \tag{49}$$

All these matrices commute approximately. Therefore, both the total and the partial cross sections for different processes can be calculated by diagonalizing the matrices $\chi_i(s,B)$.

It proves useful to introduce the following linear combinations

$$\begin{aligned} \chi^{(1)} &= a_B(q\bar{q},p\to q\bar{q},p) + a_B(q\bar{q}^\star,p\to q\bar{q},p) - a_B(q\bar{q},p^\star\to q\bar{q},p) - a_B(q\bar{q}^\star,p^\star\to q\bar{q},p) \\ \chi^{(2)} &= a_B(q\bar{q},p\to q\bar{q},p) - a_B(q\bar{q}^\star,p\to q\bar{q},p) + a_B(q\bar{q},p^\star\to q\bar{q},p) - a_B(q\bar{q}^\star,p^\star\to q\bar{q},p) \\ \chi^{(3)} &= a_B(q\bar{q},p\to q\bar{q},p) - a_B(q\bar{q}^\star,p\to q\bar{q},p) - a_B(q\bar{q},p^\star\to q\bar{q},p) + a_B(q\bar{q}^\star,p^\star\to q\bar{q},p) \\ \chi^{(4)} &= a_B(q\bar{q},p\to q\bar{q},p) + a_B(q\bar{q}^\star,p\to q\bar{q},p) + a_B(q\bar{q},p^\star\to q\bar{q},p) + a_B(q\bar{q}^\star,p^\star\to q\bar{q},p). \end{aligned} \tag{50}$$

The elastic amplitude in impact parameter representation then reads

$$\langle\gamma,p|\; a(s,B)\;|\gamma,p\rangle = Z_3\;\chi_{dir}(s,B)$$

$$+ \quad \frac{e^2}{4}\left(\frac{1}{f_{q\bar{q}}}+\frac{1}{f_{q\bar{q}^\star}}\right)^2\left\{\left(1-e^{-\chi^{(1)}(s,B)}\right)+\left(1-e^{-\chi^{(4)}(s,B)}\right)\right\}$$

$$+ \quad \frac{e^2}{4}\left(\frac{1}{f_{q\bar{q}}}-\frac{1}{f_{q\bar{q}^\star}}\right)^2\left\{\left(1-e^{-\chi^{(2)}(s,B)}\right)+\left(1-e^{-\chi^{(3)}(s,B)}\right)\right\}. \qquad (51)$$

The amplitudes necessary to calculate low mass diffractive processes are given by:

$$\langle q\bar{q}^\star, p|\ a(s,B)\ |\gamma,p\rangle =$$

$$+ \quad \frac{e}{4f_{q\bar{q}}}\left\{-e^{-\chi^{(1)}(s,B)}+e^{-\chi^{(2)}(s,B)}+e^{-\chi^{(3)}(s,B)}-e^{-\chi^{(4)}(s,B)}\right\}$$

$$+ \quad \frac{e}{4f_{q\bar{q}^\star}}\left\{4-\left(e^{-\chi^{(1)}(s,B)}+e^{-\chi^{(2)}(s,B)}+e^{-\chi^{(3)}(s,B)}+e^{-\chi^{(4)}(s,B)}\right)\right\} \qquad (52)$$

$$\langle q\bar{q}, p^\star|\ a(s,B)\ |\gamma,p\rangle =$$

$$+ \quad \frac{e}{4f_{q\bar{q}}}\left\{+e^{-\chi^{(1)}(s,B)}-e^{-\chi^{(2)}(s,B)}+e^{-\chi^{(3)}(s,B)}-e^{-\chi^{(4)}(s,B)}\right\}$$

$$+ \quad \frac{e}{4f_{q\bar{q}^\star}}\left\{+e^{-\chi^{(1)}(s,B)}+e^{-\chi^{(2)}(s,B)}-e^{-\chi^{(3)}(s,B)}-e^{-\chi^{(4)}(s,B)}\right\} \qquad (53)$$

$$\langle q\bar{q}^\star, p^\star|\ a(s,B)\ |\gamma,p\rangle =$$

$$+ \quad \frac{e}{4f_{q\bar{q}}}\left\{+e^{-\chi^{(1)}(s,B)}+e^{-\chi^{(2)}(s,B)}-e^{-\chi^{(3)}(s,B)}-e^{-\chi^{(4)}(s,B)}\right\}$$

$$+ \quad \frac{e}{4f_{q\bar{q}^\star}}\left\{+e^{-\chi^{(1)}(s,B)}-e^{-\chi^{(2)}(s,B)}+e^{-\chi^{(3)}(s,B)}-e^{-\chi^{(4)}(s,B)}\right\}. \qquad (54)$$

The cut amplitudes which enter the calculation of high mass single diffraction can be written as

$$\langle \gamma_{had}, p|\ \left(-2\chi_{TP,a}(s,B)\right)e^{-2\chi(s,B)}\ |\gamma_{had},p\rangle =$$

$$\frac{e^2}{4}\left(\frac{1}{f_{q\bar{q}}}+\frac{1}{f_{q\bar{q}^\star}}\right)^2\left[\left(-2\chi^{(1)}_{TP,a}\right)e^{-2\chi^{(1)}} \quad + \quad \left(-2\chi^{(4)}_{TP,a}\right)e^{-2\chi^{(4)}}\right]$$

$$\frac{e^2}{4}\left(\frac{1}{f_{q\bar{q}}}-\frac{1}{f_{q\bar{q}^\star}}\right)^2\left[\left(-2\chi^{(2)}_{TP,a}\right)e^{-2\chi^{(2)}} \quad + \quad \left(-2\chi^{(3)}_{TP,a}\right)e^{-2\chi^{(3)}}\right] \qquad (55)$$

Here the index a labels the diffractively dissociating particle γ_{had} or p, respectively. The eikonal functions $\chi^{(i)}_{TP,a}$ are linear combinations of the triple Pomeron amplitudes $a_{TP,a}$ which are analogous to Eq. (50). By substituting the loop Pomeron amplitude for the triple Pomeron amplitude in Eq. (55) one gets a similar expression relevant for high mass double diffraction.